June 1969

High-Field Galvanomagnetic Properties of $AuAl_2$, $AuGa_2$, and $AuIn_2$

J.T. Longo
Department of Physics, Michigan State University, East Lansing, Michigan

P.A. Schroeder
Department of Physics, Michigan State University, East Lansing, Michigan

David J. Sellmyer
University of Nebraska-Lincoln, dsellmyer@unl.edu

High-Field Galvanomagnetic Properties of $AuAl_2$, $AuGa_2$, and $AuIn_2$†

J. T. LONGO* AND P. A. SCHROEDER††
Department of Physics, Michigan State University, East Lansing, Michigan 48823
AND
D. J. SELLMYER§
Center for Materials Science and Engineering, Massachusetts Institute of Technology, Cambridge, Massachusetts 02139
(Received 29 October 1968; revised manuscript received 24 January 1969)

Measurements of the magnetoresistance and Hall voltage have been made in the high-field region on the metallic fluorite compounds $AuAl_2$, $AuGa_2$, and $AuIn_2$. The results have been compared with those expected from the nearly-free-electron (NFE) model. These compounds are uncompensated. The magnetoresistance measurements in principal planes and directions, with one exception, support the NFE model, but the dimensions of the two-dimensional areas of aperiodic open orbits show pronounced deviations. Hall-effect measurements for **B** in the ⟨100⟩ and ⟨111⟩ directions indicate significant departures of the real Fermi surface from the NFE model. A proposed empirical model gives much better agreement with Hall-effect, magnetoresistance, and de Haas–van Alphen measurements. In the best $AuGa_2$ crystal, magnetoresistance whiskers have been observed and classified in some detail. The magnetoresistance has been calculated for **B** in the {100} plane, assuming a constant relaxation time and a model of the fourth electron zone with a topography similar to the NFE Fermi surface.

I. INTRODUCTION

UNTIL recently, measurements of the high-field galvanomagnetic properties of metals have been confined to the elements. However, in the past few years, such measurements have assisted in investigations of the Fermi-surface topologies of several intermetallic compounds.[1–5] These investigations have been successful because the high-field condition $\omega_c\tau \gg 1$ for all carriers (ω_c is the cyclotron frequency and τ is the relaxation time for electron scattering), can be approached by using magnetic fields $\sim$100 kG and single crystals with residual resistance ratios [RRR$\equiv\rho$(295°K)/ρ(4.2°K)]$>$100.

The first report on high-field magnetoresistance in the metallic fluorite compounds AuX_2 (X=Al, Ga, In) concentrated on $AuAl_2$ crystals with RRR up to 550.[4] Since then we have succeeded in growing $AuGa_2$ crystals with RRR up to 900. This has made possible the comprehensive comparison of the galvanomagnetic properties and Fermi-surface topology of these two compounds. Because of the lower quality of our $AuIn_2$ samples, only qualitative conclusions can be reached concerning its Fermi surface.

Band-structure calculations have not yet been made on these fluorite compounds. [*Note added in proof.* Since time of writing A. C. Switendick has performed augmented plane wave calculations of the band structures. Bull. Am. Phys. Soc. **14**, 360 (1969).] In this paper, we therefore concentrate on comparing our experimental results with those of the nearly-free-electron (NFE) model and suggesting ways in which the latter must be modified to fit the data.

The fluorite compounds AuX_2 are of considerable interest, since differences among their Fermi surfaces must be explicable in terms of the differing atomic potentials at the X sites. The NFE model of the Fermi surface ignores this feature since it assumes an "empty lattice." On the basis of the pseudopotential cancellation theory[6] one would expect that $AuAl_2$ should be the least and $AuIn_2$ the most NFE-like, since energy gaps separating the conduction bands should be a decreasing function of the atomic number of the X atom. This effect has already been noted to occur in the energy gaps separating the valence and conduction bands of elements in the fourth column of the periodic table and in the compounds InX (X=P, As, Sb, Bi) and Mg_2X (X=Si, Ge, Sn, Pb).[7] de Haas–van Alphen (dHvA) data on AuX_2 have validated use of the NFE model as a first approximation, but do not generally show the above trend.[8]

In Sec. II, we briefly discuss the theory of high-field galvanomagnetism and present the NFE model of the Fermi surface. Section III is concerned with sample preparation and measurement techniques. In Sec. IV, we present our magnetoresistance results followed by our Hall-effect measurements. Finally, in Sec. V, we compare these results with those predicted by the NFE

† Work performed in part at the Francis Bitter National Magnet Laboratory which is supported by the U. S. Air Force Office of Scientific Research.
* Present address: Science Center, North American Rockwell Corp., Thousand Oaks, Calif.
†† Supported by the National Science Foundation.
§ Supported by the Advanced Research Projects Agency.
[1] D. J. Sellmyer and P. A. Schroeder, Phys. Letters **16**, 100 (1965).
[2] J. Piper, J. Phys. Chem. Solids **27**, 1907 (1966).
[3] D. J. Sellmyer, J. Ahn, and J. P. Jan, Phys. Rev. **161**, 618 (1967).
[4] J. T. Longo, P. A. Schroeder, and D. J. Sellmyer, Phys. Letters **25A**, 747 (1967).
[5] J. Ahn and D. J. Sellmyer, Bull. Am. Phys. Soc. **13**, 485 (1968).
[6] P. W. Anderson, *Concepts in Solids* (W. A. Benjamin, Inc., New York, 1963), p. 71.
[7] D. J. Sellmyer, Ph.D. thesis, Michigan State University, 1965 (unpublished).
[8] J. P. Jan, W. B. Pearson, Y. Saito, M. Springford, and I. M. Templeton, Phil. Mag. **12**, 1271 (1965).

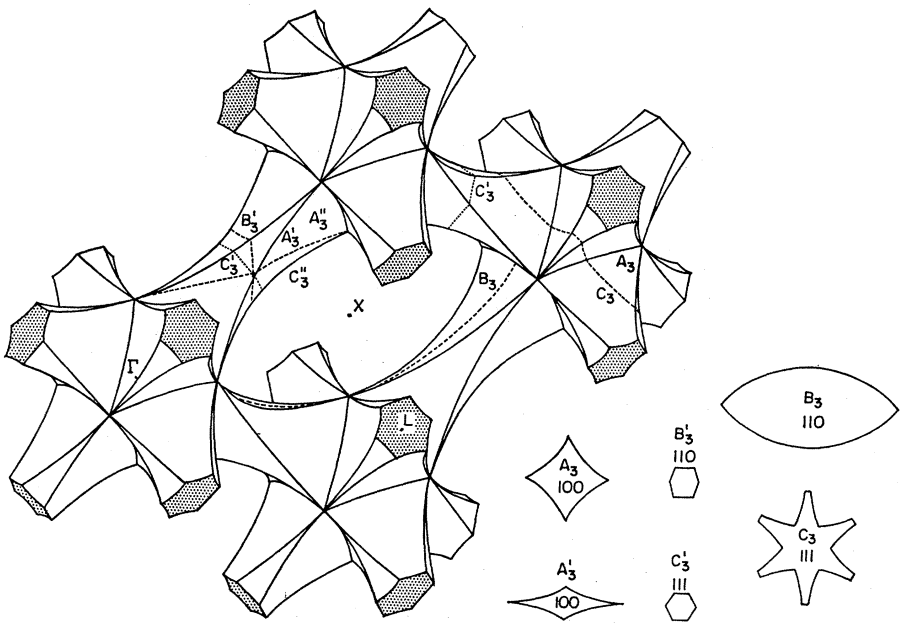

FIG. 1. Holes in the third-zone, NFE model, repeated zone scheme [after Jan *et al.* (Ref. 8)].

model and suggest how the NFE Fermi surface must be modified. In the Appendix, we give the outline and results of a calculation of the magnetoresistance for **B** in the {100} plane for an open Fermi surface with topology and dimensions similar to the fourth zone of the NFE model.

II. THEORY

A. High-Field Galvanomagnetic Effects

The results of Lifshitz, Azbel', and Kaganov[9] which are pertinent to this study are given in Table I. Ω is the volume of the primitive cell in the direct lattice, β is the complement of the angle between **J** and **B**, and **J** makes angle α with the open orbit directions. From the Hall effect for **B** in a direction where there are no open orbits, we can find n_e-n_h. (n_e and n_h are the number of occupied electron and hole states, respectively, in partially filled bands per primitive cell of the crystal.) From the Hall effect in a singular direction we can find Δn. This is a correction term which arises from the presence of hole orbits on an electron sheet, and vice versa, for **B** in a singular direction. It is easy to evaluate for a given Fermi-surface model:

$$\Delta n=\left(\frac{2\Omega}{2\pi\hbar}\right)^3\int_{-d/2}^{d/2}A(p_z)dp_z,$$

where $A(p_z)$ is the cross-sectional area of the Brillouin zone for crystal momentum p_z in a direction parallel to the magnetic field **B**. The quantity d is the p_z width over which the orbits have a character opposite to that of the open sheet.

[9] I. M. Lifshitz, M. Ya. Azbel', and M. I. Kaganov, Zh. Eksperim. i Teor. Fiz. **31**, 63 (1956) [English transl.: Soviet Phys.—JETP **4**, 41 (1957)].

B. NFE Model of Fermi Surface

Figures of the surfaces of the NFE model in zones 2–6 are available in the literature.[8] These are based on the assumption that gold contributes one electron and the polyvalent element three electrons per atom to the conduction band. We reproduce in Figs. 1 and 2 the multiply connected zones 3 (holes) and 4 (electrons) with which we are primarily concerned. Subscripted letters refer to orbits enclosing maximal or minimal cross-sectional areas. Sufficient dHvA frequencies corresponding with these areas have been observed[8] to confirm that the NFE Fermi surface is a good first approximation to the true Fermi surface.

C. Calculation of Magnetoresistance

In these AuX_2 compounds, we have observed a very large magnetoresistance (compared with copper, for example) for relatively small values of $\omega_c\tau$. To under-

TABLE I. Summary of high-field galvanomagnetic properties. The Hall field is the transverse electric field for unit current density; β is the complement of the angle between **J** and **B**; **J** makes an angle α with the open orbit direction.

Type of orbit and state of compensation	Magneto-resistance	Hall field
(1) All closed and uncompensated ($n_e\neq n_h$)	$\sim B^0$	$\dfrac{-\Omega B}{(n_e-n_h)\lvert e\rvert\cos\beta}$
(2) All closed and compensated ($n_e=n_h$)	$\sim B^2$	$\sim B$
(3) Open in one direction	$\sim B^2\cos^2\alpha$	$\sim B$
(4) Open in two directions	$\sim B^0$	$\sim B^{-1}$
(5) Singular field direction	$\sim B^0$	$\dfrac{-\Omega B}{(n_e-n_h\mp\Delta n)\lvert e\rvert\cos\beta}$

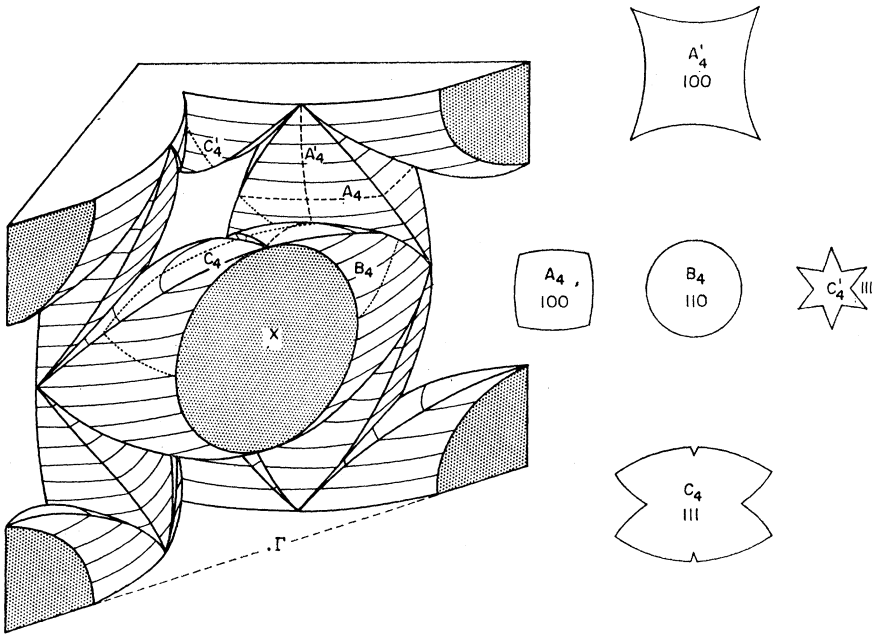

FIG. 2. Fourth-zone, electron surface, NFE model [after Jan *et al.* (Ref. 8)].

stand this, we have extended the single relaxation time model of Coleman *et al.*[10] to cover more complicated Fermi surfaces. This extension and calculation of the magnetoresistance in the {100} plane for an open Fermi surface with topology and dimensions similar to that of the fourth zone of the NFE model are given in the Appendix. In this calculation, we assumed that the holes and electrons in the second, third, fifth, and sixth zones could be treated as free carriers. Justification of this assumption, especially for the third-zone holes, is given in the Appendix. The result is that for $\omega_c\tau \gtrapprox 10$ the magnetoresistance

$$\Delta\rho/\rho = 2n\zeta(\omega_c\tau)^2 - 1.$$

The calculated angular dependence of ζ is given in the Appendix. n is the number of conduction electrons per primitive cell. The large magnetoresistances observed (up to 500) result both from the factor n which has the value 7 for the AuX_2 compounds compared with 1 for copper, and from the term ζ which is less than 0.7 for AuX_2 and less than 0.1 for copper.

Another interesting point which arises out of this calculation is that the magnetoresistance is proportional to the p_z thickness of the layers of open orbits only when a small fraction of the total carriers are on open orbits. This is further discussed in the Appendix.

III. EXPERIMENTAL

A. Apparatus

The apparatus used in these experiments has already been described.[3,11] It has two degrees of freedom so that the crystallographic axes may be rotated to make any desired angle with the field. This is illustrated in Fig. 3. The angle φ measures the deviation of **J** from the plane perpendicular to **B** when $\psi = 0°$. The angle ψ measures the rotation of the crystal about an axis described by **J** (when $\varphi = 0°$) and is continuously variable.

B. Sample Preparation

For each of the compounds, the highest resistance-ratio samples were obtained by initially melting and mixing the components in an alumina crucible by induction heating, and thereafter lowering the samples once through a three-turn rf coil. Zone refining generally did not improve the resistance ratio. Indeed, it appeared that the best samples contained a slight excess of X. This may be connected with the large concentration of vacancies which these materials apparently contain. Straumanis and Chopra[12] have determined that the extent of the $AuAl_2$ phase is 66.10–67.74 at.% Al. At the stoichiometric composition, there are 0.152 empty lattice sites per unit cell in the Al sublattice and 0.076 empty lattice sites in the Au sublattice. At the Al-rich border, there is strong evidence that all of the Al vacancies are filled. If these vacancies exist in our samples, it is clear that they must exist in the form of voids, since the above concentration of isolated vacancies would not permit the high observed resistance ratios—unless the vacancies were ordered.[13] No superlattice lines corresponding to an ordering of vacancies have been observed.[14]

[10] R. V. Coleman, A. J. Funes, J. S. Plaskett, and C. M. Tapp, Phys. Rev. **133**, A521 (1964).
[11] D. J. Sellmyer, Rev. Sci. Instr. **38**, 431 (1967).
[12] M. E. Straumanis and K. S. Chopra, Z. Physik. Chem. Neue Folge **42**, 344 (1964).
[13] G. T. Meaden, *Electric Resistance of Metals* (Plenum Press, Inc., New York, 1965), p. 123.
[14] M. E. Straumanis (private communication).

The fact that the number of vacancies decreased as the Al-rich phase boundary was approached suggested that better resistance ratios may be obtained for an excess of Al. In fact, all the crystals used in this research were prepared at the Al-rich border of the phase and had RRR$\approx$500. $AuAl_2$ crystals prepared with stoichiometric proportions and zone refined had RRR$\approx$140. The preparation of $AuAl_2$ is difficult because it wets the alumina crucible and all other crucible materials tried to date.

For $AuGa_2$ for which no details of the phase are available, slugs of 0.0, 0.1, 0.2, 0.3, 0.4, and 0.5 wt% excess Ga were prepared. The average RRR of crystals cut from these slugs were 190, 540, 680, 710, 660, and 200, respectively, with considerable spread about these averages. The crystals have not been chemically analyzed to determine whether they contain the excess Ga which was originally added to the mixture of components. In fact, traces of Ga were found on the surfaces of slugs with 0.2–0.5 wt% excess Ga, so that the composition is almost certainly different.

C. Measuring Techniques

All the data presented were taken at the Francis Bitter National Magnet Laboratory in fields up to 150 kG. Throughout, it was essential to perform the usual reversals of current and field to obtain the Hall data independent of thermal emf's and magnetoresistance voltages arising from probe misalignment. Generally, the unwanted voltages appearing on the magnetoresistance probes were negligibly small for field directions supporting open orbits. For general field directions, however, errors in neglecting these were sometimes appreciable. Most of the magnetoresistance runs were performed without current and field reversals, but many checks were made using the rigorous reversal methods. The field dependences were investigated by two methods. First, the rotation runs were performed at two different values of $|\mathbf{B}|$. From these, it was possible to determine readily regions where $m>1.5$, the arbitrary criterion adopted to distinguish "quadratic" regions, and regions where $m<0.7$, the criterion adopted for eventual saturation. Second, for the principal crystallographic directions, and for other directions of specific interest where the first method did not give unequivocal results, the magnetoresistance was measured as a function of B at constant field direction.

IV. EXPERIMENTAL RESULTS

The data consist of some 300 plots of magnetoresistance versus B, magnetoresistance versus direction of $\mathbf{B}$, and Hall voltage versus B for specific directions of $\mathbf{B}$. Since magnetoresistance data are commonplace now, we present the results of our data in final stereographic and table form and show original data only where they are of specific interest.

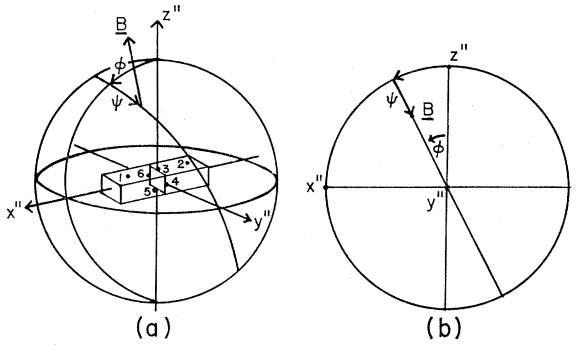

FIG. 3. (a) Rotation and tipping geometry in the sample coordinate system. Magnetoresistance leads are connected at 1 and 2, Hall leads at 3–6. (b) Stereogram showing the effect in the sample coordinate system of rotating and tipping the sample n the magnetic field.

A. Magnetoresistance Results

We first present evidence which indicates how effectively we are in the high-field region for which $\omega_c\tau\gg1$.

(I) From the free-electron model we estimate $\omega_c\tau\approx5$ for $AuAl_2$ crystals with RRR=500 at 150 kG. For $AuGa_2$ crystals with RRR=475 and 725 we estimate $\omega_c\tau\approx3$ and 6, respectively.

(II) We show in Fig. 4 some typical plots of magnetoresistance versus B for $AuGa_2$ with RRR=725. These are representative of the $AuGa_2$ and $AuAl_2$ results. For $\mathbf{B}$ in the {100} plane, the magnetoresistance exhibits a field dependence close to quadratic; $(\Delta\rho/\rho)\alpha\ B^m$ with the exponent $m=1.8$. For the direction ⟨100⟩, the experimental value of $m=0$, the value expected theoretically for a singular direction. We discuss the third curve in Fig. 4 later in this section.

(III) The exponent m for the longitudinal magnetoresistance is always ≈0 at 150 kG, as predicted by theory.

(IV) In the data for our best $AuGa_2$ crystals, fine structure (whiskers) corresponding to the excitation of higher-order open orbits has been observed. These are normally observed in crystals in which $\omega_c\tau\gg1$.

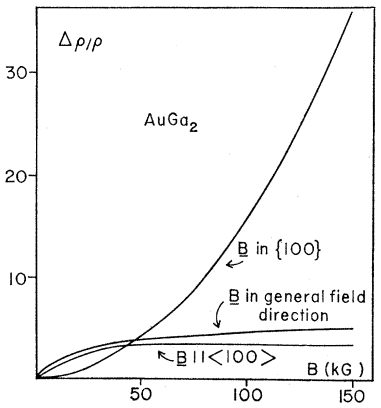

FIG. 4. $\Delta\rho/\rho$ versus B for various directions of $\mathbf{B}$.

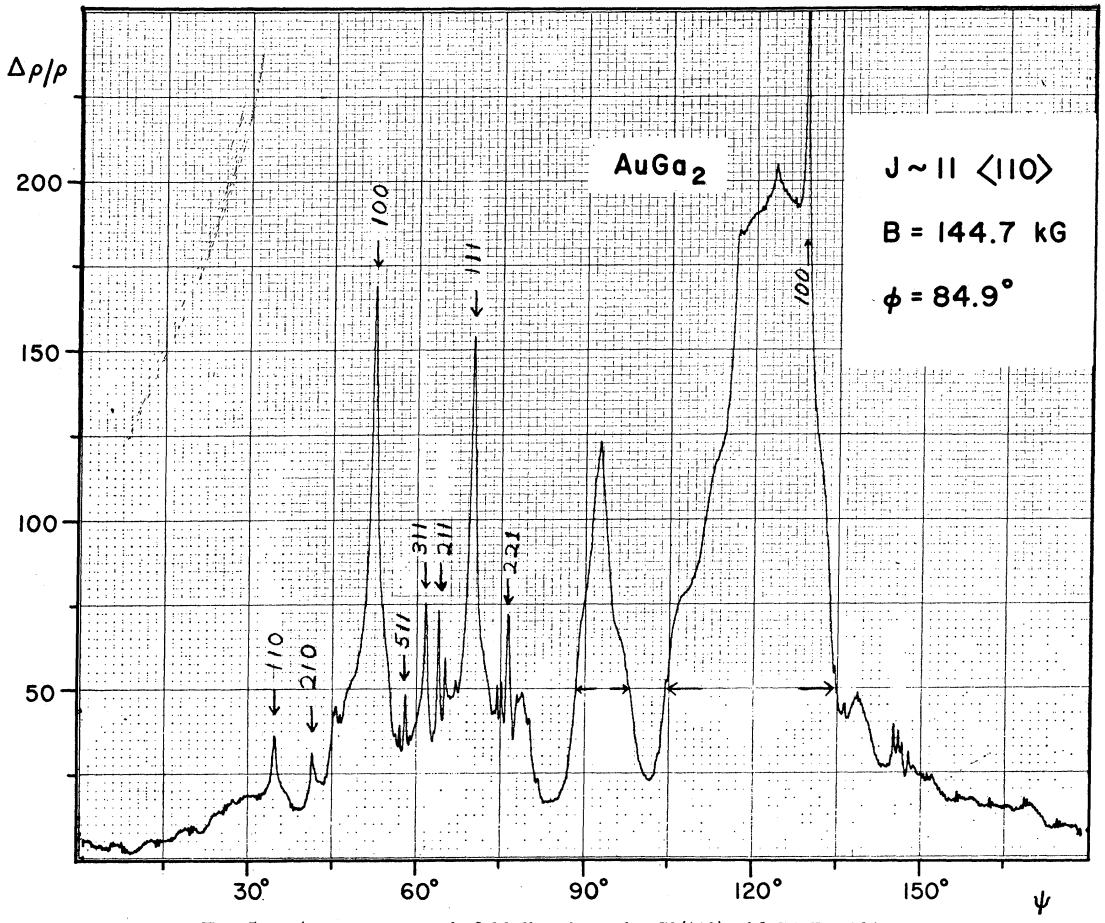

FIG. 5. $\Delta\rho/\rho$ versus magnetic field direction ψ for $G3\langle 110\rangle$ with RRR=904.

In Fig. 5 we show a typical plot of magnetoresistance versus ψ for the $AuGa_2$ sample with the highest RRR. Two-dimensional regions of open orbits centered on $\langle 111\rangle$ and $\langle 110\rangle$ produce the broad peaks (horizontal arrows). A very sharp peak is observed when B crosses $\{100\}$ at $\psi\approx 130°$. The remaining fine structure is largely the result of higher-order open orbits, for which some directions are shown in the figure. The complete list of directions starting from the left-hand side of Fig. 5 is $\langle 110\rangle$, $\langle 210\rangle$, $\langle 310\rangle$, $\langle 511\rangle$, $\langle 100\rangle$, $\langle 611\rangle$, $\langle 511\rangle$, $\langle 311\rangle$, $\langle 211\rangle$, $\langle 533\rangle$, $\langle 322\rangle$, $\langle 111\rangle$, $\langle 553\rangle$, $\langle 774\rangle$, $\langle 221\rangle$, and $\langle 331\rangle$. The results of several similar rotations with φ varying between 60° and 90° is shown in Fig. 6. The lengths of the whiskers in these figures were determined by noticing the disappearance of a peak as φ is changed. The assignment of the (774) and (553) whiskers in Fig. 6 must be considered tentative since the planes $\{332\}$ and $\{443\}$ are within 1° of the position of **B** on the stereogram where the magnetoresistance peaks occur. However, the data are sharp enough so that we estimate a maximum error of $\pm 0.5°$ in ψ, which gives considerable weight to our assignment.

The whiskers are very sensitive to the shape of the Fermi surface and have been used in the case of copper to decide which of two analytical Fermi surfaces is superior.[15] A detailed interpretation of these whiskers is not possible on the basis of the rather crude NFE model. Therefore, until serious energy-band calculations are performed on these compounds, the results presented here serve primarily as an indicator of the large values of $\omega_c\tau$ achievable in an intermetallic compound crystal.

The above observations are all consistent with high-field conditions being achieved. However, there is evidence that for some field directions there are some carriers which are still not in the high-field region for $B=150$ kG. These carriers we attribute to large extended orbits which have high cyclotron masses associated with them. For example, in Fig. 4 the results for **B** in a general field direction show incomplete saturation; $m=0.2$ at $B=150$ kG. These carriers also affect the Hall-effect measurements, as will be discussed in Sec. IV B. With the qualification that care in interpretation may be necessary where the presence of large extended orbits is suspected, we believe that the above evidence justifies our use of the high-field expressions of Table I hereafter.

[15] J. R. Klauder, W. A. Reed, G. F. Brennert, and J. E. Kunzler, Phys. Rev. 141, 592 (1966).

The graph in Fig. 4 for **B** in a general field direction, where open orbits are not anticipated, is important for another reason. The close approach to saturation indicates clearly that $AuAl_2$ is an uncompensated metal. Similar evidence confirms that this is true for $AuGa_2$ and $AuIn_2$.

In Fig. 7(a) we show the magnetoresistance plotted as a function of field direction for **B** in the {100} plane for $AuAl_2$, $AuGa_2$, and $AuIn_2$ with RRR=500, 475, and 60, respectively. We estimate that **B** does not deviate from (100) by more than 0.5° for the $AuAl_2$ and $AuGa_2$ curves. Plots of $\Delta\rho/\rho$ versus B for **B** in (100) indicate that there is a quadratic dependence throughout except at the singular direction ⟨100⟩. Earlier measurements[4] indicating discrepancies from a B^2 dependence at high fields resulted from inexact orientation of the crystal. This caused the excitation of extended open orbits which gradually took on their true closed nature only at high fields. This effect is illustrated by comparing Figs. 7(a) and 7(b) for which φ is changed by 0.6°. The numbers shown in Fig. 7(b) are the exponents m at various field directions. They frequently fall far below the value expected for a region of quadratic field dependence.

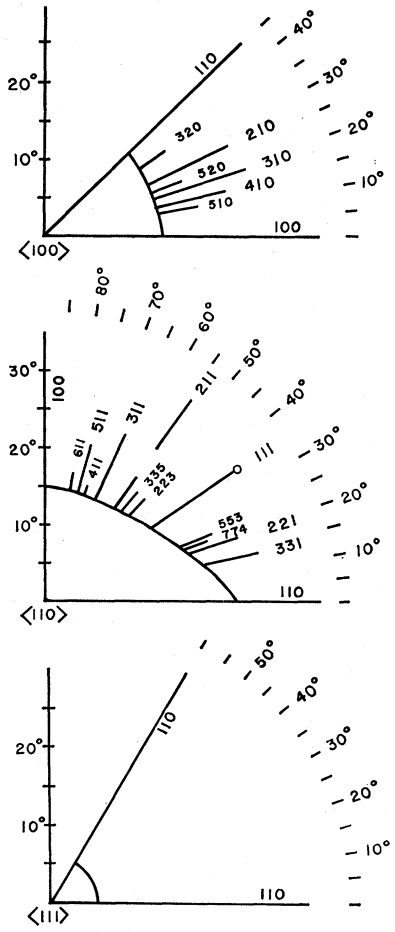

FIG. 6. "Whiskers" and two-dimensional regions in $AuGa_2$.

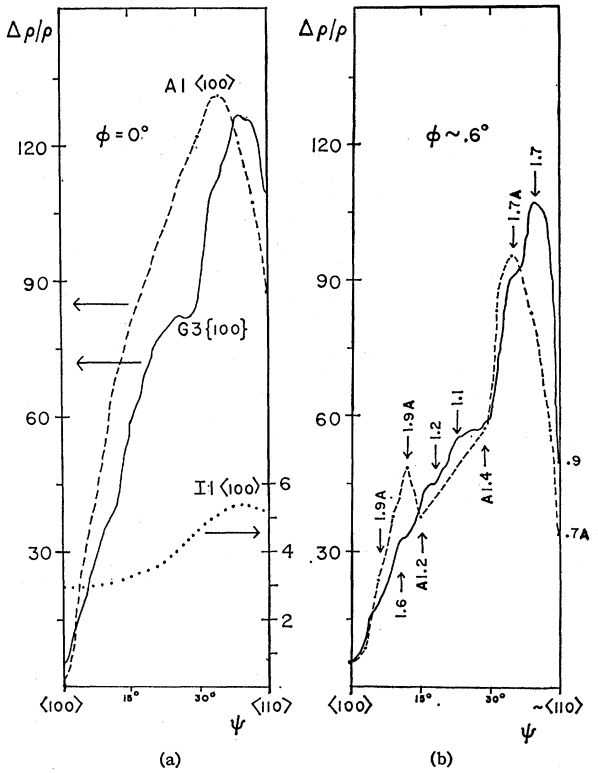

FIG. 7. (a) $\Delta\rho/\rho$ versus ψ for all three compounds for **B** in the {100} plane $B=140$ kG. (b) $\Delta\rho/\rho$ versus ψ with ϕ changed by 0.6° from (a), for $AuAl_2$ (dashed line) and $AuGa_2$ (heavy line). Values of the exponent m are shown for various field directions. Exponents labeled A refer to $AuAl_2$.

The field dependence in the vicinity of ⟨110⟩ depends very sensitively on the crystal orientation. Exponents m with values from 0.25 to 1.5 have been measured. Again, contrary to results in an earlier publication, we believe that results for **B** accurately parallel to ⟨110⟩ are quadratic in B.

For **B**∥⟨111⟩, ⟨100⟩, and ⟨211⟩, the magnetoresistance saturates in all three compounds.

From a large number of rotation and field plots similar to those illustrated in Figs. 5, 4, and 7, we have produced in Fig. 8 the stereogram showing the two-dimensional areas of aperiodic open orbits. In the experimental stereograms an open circle represents "saturation," taking the arbitrary criterion $\Delta\rho/\rho=B^m$, $m<0.7$; a solid line or dot represents the extent of quadratic field dependence, $m>1.5$. Intermediate or unknown values of m are not marked. The data shown in Figs. 8(b) and 8(c), respectively, are for $AuAl_2$, crystal axis in ⟨100⟩ and RRR=550, and $AuGa_2$, crystal axis in ⟨100⟩ and RRR=725.

The shaded two-dimensional regions are based on data taken from these and several other crystals, including rather unequivocal results from the best $AuGa_2$ sample with the crystal axis along ⟨110⟩ and RRR=900.

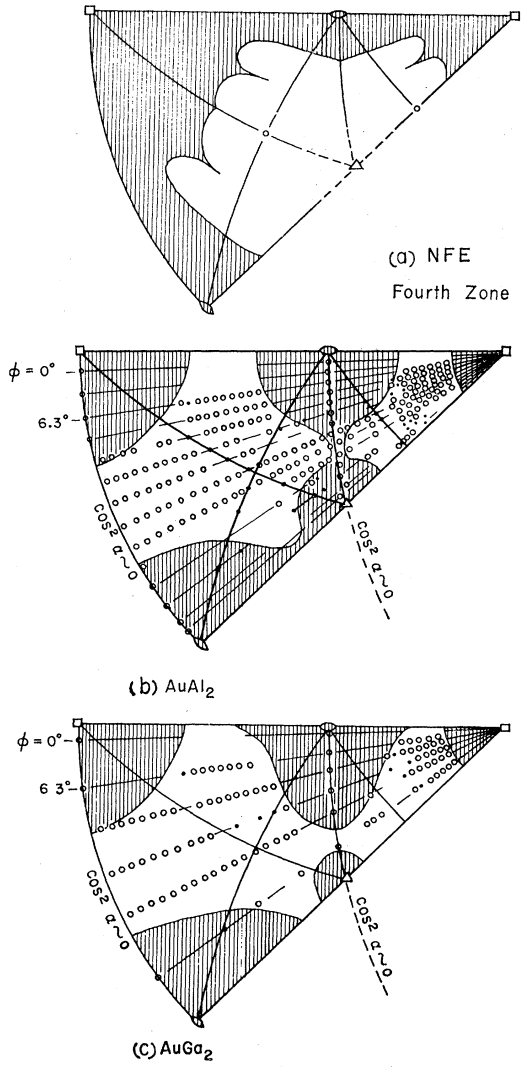

FIG. 8. (a) Magnetoresistance stereogram for the NFE model (Sec. V A) in the fourth zone. Shaded area is two-dimensional region of aperiodic orbits. Heavy line indicates one-dimensional region of periodic orbits. (b) and (c) Magnetoresistance stereograms for $AuAl_2$ ($A1\langle 100\rangle$) and $AuGa_2$ ($G3\langle 100\rangle$), respectively. Bars and dots indicate $m>1.5$; open circles mean $m<0.7$. Planes for which $\cos^2\alpha=0$ when **J** is $\langle 100\rangle$ are indicated.

We were unable to measure the two-dimensional regions of open orbits in $AuIn_2$ because of the low RRR of our samples.

B. Hall-Effect Results

We consider first the Hall-effect results for **B** in a general field direction in which no open orbits are anticipated, and for which the magnetoresistance approaches saturation.

In Fig. 9, we show the Hall voltage V_H for $AuAl_2$ with RRR=550 plotted against B for four such directions. According to Table I, the Hall voltage should be proportional to B in the high-field region, and the extrapolated linear region should pass through the origin. In Fig. 9, we have shifted the Hall-voltage curves vertically until the tangents at 150 kG passes through the origin. The theory further predicts that for the particular crystals on which the measurements of Fig. 9 were taken, $V_H=-8.0/(n_e-n_h)\ \mu V$ at $B=150$ kG. n_e-n_h can be calculated from this expression, and the intercept of the shifted curves with the $B=150$-kG axis, on the assumption that the high-field region has been reached. Theoretical values of V_H for $n_e-n_h=+1$ and $n_e-n_h=+2$ are shown in Fig. 8. In Table II we list n_e-n_h for both $AuAl_2$ and $AuGa_2$.

TABLE II. Hall data for general field directions. G and A refer to $AuGa_2$ and $AuAl_2$, respectively. The crystal axis lies in or along the plane or direction indicated.

Crystal designation	m	n_e-n_h
NFE	0.00	1.00
$G3\ \langle 100\rangle$	0.20	0.98
$G3\ \{100\}$	0.51	1.13
	0.42	1.25
	0.74	1.01
$A2$ (nonsymmetry)	0.38	0.81
	0.89	1.15
	0.50	0.99
	0.25	0.95

It is clear from both Fig. 9 and Table II that n_e-n_h is close to the value $+1$. There are significant departures from this value, however. We believe that these departures are connected with the incomplete saturation of the magnetoresistance (discussed in Sec. IV A) and the hypothesis that some carriers are still not in the high-field region. The signs of the deviations from unity indicate whether such carriers are electrons or holes.[16] Thus, in $AuAl_2$ electrons generally appear to be the lower mobility carriers, while in $AuGa_2$ the situation is reversed. The fact that $n_e-n_h\approx 1$ confirms the conclusion that these are uncompensated metals.

We now consider the Hall-effect results for **B** along $\langle 100\rangle$, $\langle 111\rangle$. The Hall voltage varies linearly with B and has a magnitude which corresponds with nonintregal values of n_e-n_h. This combined with the saturation of the magnetoresistance in those directions indicates that these are singular directions. Values of

TABLE III. Hall data for **B** in $\langle 100\rangle$ and $\langle 111\rangle$; $n=n_e-n_h\mp\Delta n$. I refers to $AuIn_2$. n_{111} for $AuIn_2$ is only tentative; the high-field conditions are probably not satisfied.

	m	n_{100}	m	n_{111}
NFE	0.0	−0.372	0.0	1.035
$I2\langle 110\rangle$	0.57	−0.68	1.08	(1.34)
$G3\{100\}$	0.32	−0.63		
$G3\langle 110\rangle$	0.0	−0.62	0.48	0.89
$G3\langle 100\rangle$	0.38	−0.68	0.50	0.92
$A1\langle 100\rangle$	0.43	−0.79	0.36	0.57

[16] E. Fawcett, Advan. Phys. 13, 139 (1964).

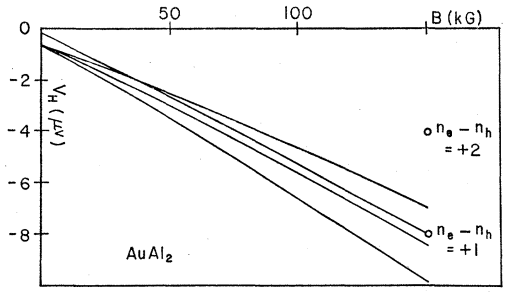

FIG. 9. Hall voltage versus B for **B** in general field directions where no open orbits are anticipated. The curves are shifted vertically until the tangents at 150 kG pass through the origin.

n_{111}, n_{100}, $(n=n_e-n_h\mp\Delta n)$ and the corresponding values of the exponent m are given in Table III. Despite the finite values of m, we are confident that the values of n_{111} and n_{100} are close to the true values for the following reasons. The values for several different crystals lie within the experimental error of $\pm 5\%$. There is no question of any discrepancy arising from extended orbits as there was for **B** in the nonsymmetry directions. The values of m are generally smaller than those for **B** in nonsymmetry directions, and finally and most significantly the Hall voltage varies linearly with field for $B>50$ kG.

Since the n_{111} and n_{100} values are clearly less than 1.0, we must conclude that there are hole orbits on an electron sheet for $AuAl_2$ and $AuGa_2$ for **B**$\|\langle 111\rangle$ and $\langle 100\rangle$.

Finally, in all three compounds, the Hall voltage decreases with $|\mathbf{B}|$ for **B** in $\langle 211\rangle$. From Table I it is clear that for **B** in $\langle 211\rangle$ there are nonintersecting orbits open in two directions.

V. DISCUSSION

A. Predictions of the NFE Model

We have analyzed the NFE sheets of the Fermi surface to determine their galvanomagnetic properties with the aid of a computer program which performs the Harrison construction. In this, we again assumed that gold contributes one electron, and the polyvalent atom three electrons per atom to the conduction band. Cross

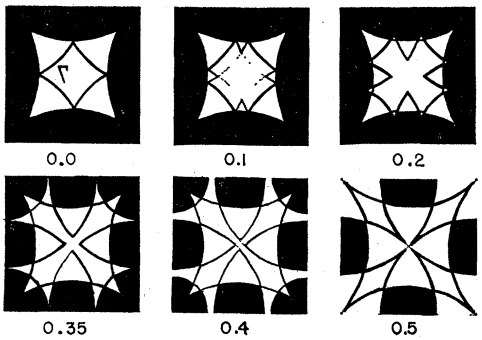

FIG. 10. Cross sections of the NFE surfaces in the third (clear) and fourth (shaded) zones at the p_z values given for **B**$\|\langle 100\rangle$. Height of the unit cell=2.

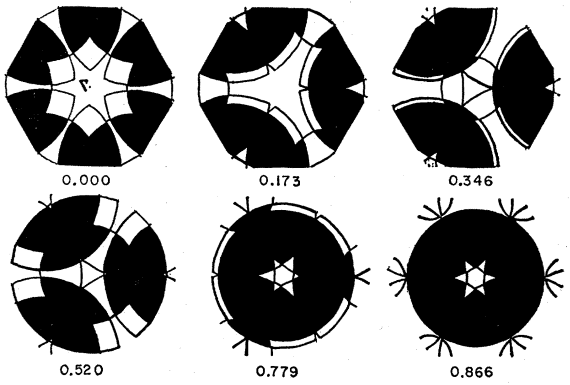

FIG. 11. As for Fig. 10, but **B**$\|\langle 111\rangle$. Height of the unit cell=0.577.

sections obtained from this construction for **B**$\|\langle 100\rangle$ and $\langle 111\rangle$ are shown in Figs. 10 and 11, respectively. In both cases, the distance of the cross section from Γ (see Figs. 1 and 2) is measured in units of $2\pi\hbar/a$, where a is the lattice parameter, so that the figures should be the same for each AuX_2 compound. With **B** in a nonsymmetry direction, it was necessary to consider a cross section through a large number of zones, usually about 25, to distinguish between extended and open orbits. Scrutiny of a larger number of zones might reveal that an open orbit was actually extended, but much larger values of $\omega_c\tau$ than we obtained would be required to discern the difference experimentally.

We can work out the state of compensation from[16]

$$n_e-n_h=n_v-2(F+J),$$

where n_v is the number of valence electrons per primitive cell of the crystal, F is the number of full zones, and J is the number of zones with hole sheets. For the NFE model this gives

$$n_e-n_h=1,$$

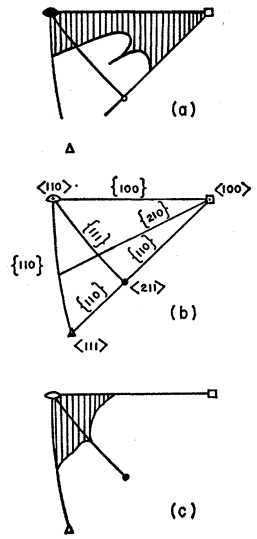

FIG. 12. (a) Magnetoresistance stereogram for the fourth zone of the NFE model. Shaded areas are two-dimensional regions of aperiodic open orbits, and the lines are one-dimensional regions of periodic open orbits. (b) Standard 100 stereogram. (c) Magnetoresistance stereogram for the third zone of the NFE model.

and a metal with the NFE topology is therefore uncompenstated. The further results of this analysis are given below and in Fig. 12.

The third zone has the following properties depending on the ⟨111⟩-directed necks.

(1) There are electron orbits on this hole surface for $\mathbf{B}\|\langle 111\rangle$ (see Fig. 11, $z=0.866$). ⟨111⟩ is therefore a singular direction. The two-dimensional region of open orbits about this direction is estimated to extend less than 1° from ⟨111⟩, because of the thinness of the electron orbit layer.

(2) There is a much larger two-dimensional region about ⟨110⟩.

(3) The surface supports primary[17] open orbits in ⟨111⟩ when **B** is in {111} and secondary open orbits in ⟨100⟩ when **B** is in {100} except for directions ⟨100⟩ and ⟨110⟩. It further supports secondary open orbits in the direction ⟨110⟩ for a limited section of the {110} plane.

dHvA data[8] for this surface indicate that the necks are decreased to $\frac{1}{3}$ of the NFE area in $AuGa_2$ and $AuIn_2$ and to 1/15 of that value in $AuAl_2$. This will, we estimate, eliminate the two-dimensional area about ⟨111⟩ because the electron orbits on this surface should vanish. Consequently, since there are no hole orbits on the fourth-zone surface for this field direction, a measurement of the Hall field for a NFE metal would indicate that the effective carrier concentration was one electron per primitive cell. The neck shrinkage will also cause a diminution of the size of the two-dimensional region about ⟨110⟩. Calculations of field directions which support open orbits on a model with a Fermi wave vector increased $\lesssim 5\%$ to give the experimentally observed area of the necks indicate that open orbits from the third zone only occur in field directions for which there are already open orbits on the fourth-zone surface.

The essential topology of the fourth-zone electron sheet is clearly indicated in the Appendix in Fig. 14. The NFE model has the following properties.

(1) For $\mathbf{B}\|\langle 110\rangle$ there are ⟨100⟩ directed open orbits.

(2) There are hole orbits on this electron sheet for $\mathbf{B}\|\langle 100\rangle$ (Fig. 10, $z=0.00$–0.343) and for $\mathbf{B}\|\langle 110\rangle$. The two-dimensional regions about these axes are connected. The rather abrupt disappearance of the aperiodic open orbits as **B** moves away from ⟨110⟩, while remaining between the planes {110} and {111}, is caused by the intersection of orbits open in different average directions. One set of orbits is derived from the ⟨100⟩ orbits seen for $\mathbf{B}\|\langle 110\rangle$; the other set arises from the unfolding of the hole orbits for $\mathbf{B}\|\langle 110\rangle$. For small angular deviations from ⟨110⟩, they combine to give orbits open in one direction.

(3) There are primary, secondary, and tertiary open orbits in ⟨100⟩, ⟨110⟩, and ⟨111⟩, respectively, for **B** in {100}, {111}, and parts of {110}. There are tertiary open orbits for **B** in ⟨210⟩.

(4) For $\mathbf{B}\|\langle 211\rangle$ there are nonintersecting open orbits in ⟨111⟩ and ⟨110⟩.

In connection with the fourth-zone two-dimensional areas, it should be noted that a model used by Lifschitz and Peschanskii,[18] with undulating cylinders along ⟨100⟩, ⟨110⟩, and ⟨111⟩, does not permit two-dimensional regions to be connected. This model cannot have general validity since the Harrison construction for our NFE model does yield connected two-dimensional regions. The Lifschitz-Peschanskii model, furthermore, does not permit nonintersecting open orbits for $\mathbf{B}\|\langle 211\rangle$ nor open orbits for $\mathbf{B}\|\langle 110\rangle$.

B. Comparison of Magnetoresistance with NFE Model

Generally, the results for principal planes and directions agree with the predictions of the NFE model outlined in Sec. V A and illustrated in Fig. 12. The one exception is that in all three compounds the magnetoresistance for **B** in {110} is quadratic unless the field is close to ⟨211⟩. On the NFE model there is no one-dimensional region of open orbits near ⟨111⟩.

We notice in particular that for $\mathbf{B}\|\langle 211\rangle$, all three compounds have the saturating magnetoresistance and a vanishing Hall voltage typical of nonintersecting orbits open in two directions as predicted by the NFE model.

In Fig. 8 we compare the ⟨100⟩ stereograms for the NFE model fourth zone with the experimentally determined stereograms for $AuGa_2$ and $AuAl_2$. We noted in Sec. V A that when the reduced size of the third zone necks (as indicated by dHvA effect) is taken into account, the two-dimensional regions of the third zone will almost certainly be all in regions covered by the two-dimensional regions of the fourth zone. We therefore do not further consider NFE predictions for the two-dimensional areas from the third zone.

The experimental results differ from the predictions of the NFE model in the following respects.

(1) The experimental two-dimensional regions about ⟨100⟩ and ⟨110⟩ are not connected.

(2) The ⟨110⟩ and ⟨111⟩ open orbit regions are probably connected in $AuAl_2$ but definitely are not in $AuGa_2$.

(3) There is some evidence that there is a two-dimensional region surrounding ⟨211⟩. ⟨211⟩ is not surrounded by aperiodic open orbits on the NFE model.

(4) There is an appreciable two-dimensional area about ⟨111⟩. With the third-zone necks size obtained from dHvA measurements, no two-dimensional area is expected.

[17] For definitions of primary, secondary, etc., open orbits, see Ref. 16, p. 144.

[18] I. M. Lifshitz and F. G. Peschanskii, Zh. Eksperim. i Teor. Fiz. 38, 188 (1960) [English transl.: Soviet Phys.—JETP 11, 137 (1960)].

C. Comparison of Hall Effect with NFE Model

There is general agreement between the value of n_e-n_h obtained from measurements of the Hall voltage in a general field direction and the experimental prediction $n_e-n_h=+1$ for the NFE model. The Harrison construction reveals that the vast majority of the fourth-zone closed electron orbits extend over several zones and have high effective masses, whereas the third-zone hole orbits have small effective masses. This should give values of n_e-n_h rather less than unity if the field is insufficiently high to produce complete saturation of the magnetoresistance. This is observed in $AuAl_2$ (Table II). We cannot explain the values of n_e-n_h rather greater than unity obtained for $AuGa_2$ in terms of the NFE model.

In Table III we compare the values of n_{100} and n_{111} obtained experimentally form Hall-effect measurements with **B** in ⟨100⟩ and ⟨111⟩, respectively, with the NFE values. The experimental values in both cases are less than the NFE values and also less than unity, indicating that the real Fermi surface must have more hole orbits on electron sheets than does the NFE Fermi surface. These orbits can only be obtained by modifying the fourth-zone sheet. Figures 10 and 11 display pertinent cross sections of the NFE model and suggest modifications which could explain our experimental results. It is clear that the cut at $p_z=0.0$ (Fig. 11) produces electron orbits in the fourth zone which are closer to contact than those of any other section. If the Fermi surface is modified so that contact is made, then the required hole orbits are automatically produced. There are two types; only the one centered at Γ is extremal. We suggest that this hole orbit produced the dHvA frequency observed in $AuAl_2$, which was assigned to the electron orbit C_4 (Fig. 2).[8] Supplementary evidence in favor of this suggestion is quite convincing. From a qualitative standpoint, an increase of electrons which causes orbits C_4 to touch explains the restricted angular extent of the dHvA frequency near ⟨111⟩, and the size of the two-dimensional region of open orbits about ⟨111⟩ observed experimentally (Fig. 8).

A similar situation exists in ⟨100⟩. In Fig. 10 we see that hole orbits exist on the fourth-zone electron sheet up to a p_z value of 0.343, whereas to explain the results they should exist for p_z values up to 0.42 in $AuIn_2$, 0.41 in $AuGa_2$, and 0.45 in $AuAl_2$.

The Hall-effect measurements in the ⟨100⟩ and ⟨111⟩ directions both suggest specific modifications of the Fermi surface. In both instances the modification corresponds with filling the deep valleys (Fig. 2) in the NFE model. In Sec. V D we present and discuss a semiquantitative model which agrees with the known experimental results much better than the NFE model. However, we first consider the possibility of salvaging the NFE model by postulating magnetic breakdown of orbits like C_4 to form the hole orbits observed. Experimental evidence discredits this postulate. Plots of Hall voltage versus magnetic field along ⟨100⟩ and ⟨111⟩ are linear to within 5% above 50 kG. Hence breakdown must be complete at this field or commence above 150 kG. If it is complete at 50 kG, the breakdown field B_0 must be of the order of 10 kG, since the probability of transition between two orbits coupled by magnetic breakdown is given by

$$P=e^{-B_0/B}, \quad B_0=K\Delta^2 m/\epsilon_F eh, \quad K\approx 1$$

and Δ is the energy gap separating two energy bands.

Now consider a simple breakdown model in which C_4 is represented by a second-zone overlap and C_3 by first-zone holes. Using the known values of the effective masses, NFE and dHvA areas of C_3 and C_4, we calculate $B_0\approx 150$ kG. Further evidence against a $B_0\approx 10$ kG is the "normal" behavior of $\Delta\rho/\rho$-versus-B curves at ⟨100⟩ and ⟨111⟩.

TABLE IV. Comparison of properties of a model with a Fermi sphere which gives experimental n_{111} values, with experimental quantities.[a] Extremal areas are in units of $(2\pi\hbar/a)^2$.

Property	$AuAl_2$ Measured value	$AuAl_2$ Modified NFE model	$AuGa_2$ Measured value	$AuGa_2$ Modified NFE model	NFE
n_{111}	0.57	0.57	0.91	0.91	1.035
n_{100}	−0.79	−0.84	−0.64	−0.72	−0.372
⟨111⟩ extremal area	1.7	≈1.4		≈1.5	$1.4=C_4$
Range of ⟨111⟩ orbit towards ⟨110⟩	≈5°	≈10°		≈5°	45°
B_4	1.15	≈1.2	(1.05)	≈1.09	0.75
A_4	0.62	≈0.81	0.60	≈0.77	0.62
A_4'	1.2	≈0.92		≈1.05	1.2

[a] Data in parentheses are preliminary results of dHvA measurements by J. T. Longo, P. A. Schroeder, M. Springford, and J. Stockton (unpublished).

D. Modified NFE Model of the Fermi Surface

The Hall data in the singular directions suggest that the NFE model should be modified by filling up the deep valleys of the Fermi surface in the fourth zone. A simple way of doing this, which permits us to perform a semiquantitative analysis, is to use the Harrison construction program with a Fermi radius increased until there are sufficient electrons in the fourth zone to give the correct n_{111} value. Notice that we do not use this model to predict properties which depend on any zone but the fourth.

For $AuGa_2$ and $AuAl_2$ the appropriate increase in Fermi radius (in units of $2\pi\hbar/a$) is from the NFE value 1.495 to 1.532 and 1.552, respectively. In Table IV we compare properties of the modified model with a variety of experimentally measured quantities. Then n_{100} values are clearly in better agreement with the modified model than with the original NFE model. The ⟨111⟩ extremal areas are roughly the same on both models, but the (hole) orbits on the modified model are quite different from the (electron) orbit C_4 of the NFE model. The angular range of the ⟨111⟩ orbit towards ⟨110⟩ in (110) is in much better agreement with the modified model, as are the B_4 areas. The results for A_4 and A_4' agree better

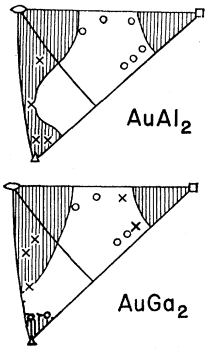

FIG. 13. Magnetoresistance stereograms comparing experimental open orbit regions (shaded) with the type of open orbit (0=closed, ×=open) predicted by the modified NFE model.

with the NFE model. Since the orbit A_4 does not pass through the valley region, and since only a small part of orbit A_4' is in the valley region, this confirms that the electrons are preferentially filling the valleys of the Fermi surface.

The next task is to see how the predictions of the modified model agree with the magnetoresistance results, particularly for the two-dimensional areas. We have studied Fermi-surface cross sections obtained from the Harrison construction with the appropriately increased Fermi wave vector for four symmetry directions and ten nonsymmetry directions of **B** for $AuGa_2$ and $AuAl_2$. In the NFE model, only one of the chosen nonsymmetry directions of **B** gives the correct experimental result. In Fig. 13 we summarize this analysis and compare it with experimental results. The shaded areas represent the experimentally determined two-dimensional regions of aperiodic open orbits taking the results of all crystals into consideration.

The agreement is excellent for $AuAl_2$. The connection of the two-dimensional regions about ⟨110⟩ and ⟨100⟩ has disappeared. The ⟨110⟩ and ⟨111⟩ regions are probably linked. At ⟨211⟩ there are still open orbits in two directions and there is a small band of hole orbits on the electron sheet. This may result in aperiodic open orbits near this axis. Finally, the model gives an appreciable two-dimensional region about ⟨111⟩.

For the $AuGa_2$ model, four of the ten nonsymmetry field directions still give erroneous results and indicate that the ⟨100⟩ two-dimensional region is too large and the ⟨111⟩ region too small. The two-dimensional areas about ⟨110⟩ and ⟨111⟩ are probably not linked, in agreement with experiment, but no hole orbits exist on the electron sheet for $\mathbf{B}\|\langle 211\rangle$.

Both the models and the magnetoresistance and Hall-effect experiments confirm that for **B** near ⟨100⟩ and ⟨111⟩ the Fermi surface for $AuGa_2$ is more NFE-like than that of $AuAl_2$.

VI. CONCLUSIONS

(1) The AuX_2 compounds are uncompensated metals with $n_e - n_h = 1$.

(2) The high-field magnetoresistance, with one exception, is in agreement with the NFE model for **B** in principal low index planes and directions.

(3) Serious discrepancies from the NFE model occur in (a) the Hall effect for **B** in the ⟨111⟩ and ⟨110⟩ directions and (b) the area of the two-dimensional regions of aperiodic open orbits.

(4) These discrepancies largely disappear in a semi-empirical model in which the Harrison construction is used with radius of the Fermi sphere increased from the NFE value of $1.495\ 2\pi\hbar/a$ to $1.552\ 2\pi\hbar/a$ for $AuAl_2$. The agreement for $AuGa_2$ with the Fermi radius increased to $1.532\ 2\pi\hbar/a$ is not quite so good but shows considerable improvement over the NFE model. As far as the galvanomagnetic properties are concerned, the critical effect of this construction is to fill the deep valleys in the NFE Fermi surface.

(5) Over-all $AuGa_2$, appears to have a Fermi surface more generally approximating the NFE model, as one would expect from the pseudopotential cancellation theory.

(6) The existence of many whiskers in the magnetoresistance indicates the high values of $\omega_c\tau$ attainable in at least some intermetallic compounds.

(7) A theoretical calculation of the magnetoresistance has been performed for **B** in the {100} plane for a model with a constant relaxation time and similar topology and dimensions to the NFE model. While this is by no means precise, it is instructive in explaining the large magnetoresistances observed and in determining the regions from which the main contributions to the magnetoresistance arise.

ACKNOWLEDGMENTS

We are indebted to the staff of the Francis Bitter National Magnet Laboratory for the use of its facilities. In particular, L. G. Rubin has been most helpful and cooperative. We are also grateful to A. Davidson for assistance in the measurements.

APPENDIX

In the presence of a magnetic field $\mathbf{B}\|\hat{z}$, carriers on a Fermi surface move on curves of constant energy and constant p_z. If we define a third variable μ describing the motion tangent to the trajectory by $d\mu = -d\mathbf{p}_{\text{tangent}}/(\mathbf{v}\times\hat{z}) = |e|Bdt$, the conductivity tensor in the single relaxation time approximation is

$$\bar{\sigma} = \frac{2e^2t}{(2\pi\hbar)^3}\int\int_{\text{F.S.}} \mathbf{v}\psi d\mu\, p_z$$

with

$$\psi(\mu) = \alpha e^{-\alpha\mu}\int_{-\infty}^{\mu} e^{\alpha\mu'}\mathbf{v}(\mu')d\mu',$$

$$\alpha m = m/|e|B\tau = 1/\omega_c\tau.$$

This result is well known.

Coleman *et al.*[10] showed that for closed orbits or periodic open orbits, ψ can be put in the form

$$\psi(\mu)=\alpha e^{-\alpha\mu}\left(\frac{1}{e^{\alpha\mu_0}-1}\int_0^{\mu_0}e^{\alpha\mu'}\mathbf{v}(\mu')d\mu'+\int_0^{\mu}e^{\alpha\mu'}\mathbf{v}(\mu')d\mu'\right),$$

where μ_0 is the period of the orbit.

They then obtained $\psi^{(0)}$ and $\psi^{(1)}$ (closed orbits) in the expansion

$$\psi(\mu)=\psi^{(0)}+\alpha\psi^{(1)}+\alpha^2\psi^{(2)},$$

$$\psi^{(0)}=\frac{1}{\mu_0}\int_0^{\mu_0}\mathbf{v}(\mu')d\mu',$$

$$\psi^{(1)}=\frac{1}{\mu_0}\int_0^{\mu_0}\mu'\mathbf{v}(\mu')d\mu'-\frac{\mu}{\mu_0}\int_0^{\mu_0}\mathbf{v}(\mu')d\mu'+\int_0^{\mu}\mathbf{v}(\mu')d\mu',$$

$$\psi^{(2)}=\frac{\mu^2}{2\mu_0}\int_0^{\mu_0}\mathbf{v}(\mu')d\mu'-\frac{\mu}{\mu_0}\int_0^{\mu_0}\mu'\mathbf{v}(\mu')d\mu'$$
$$+\frac{1}{2\mu_0}\int_0^{\mu_0}\mu'^2\mathbf{v}(\mu')d\mu'-\mu\int_0^{\mu}\mathbf{v}(\mu')d\mu'+\int_0^{\mu}\mu'\mathbf{v}(\mu')d\mu'.$$

By considering the first three terms in this expansion of ψ and considering orbits open in the x direction, we can determine $\boldsymbol{\sigma}$. For simplicity, we drop the common factor $2e^2\tau/(2\pi\hbar)^3$ and omit the integration $\int dp_z$. In the following, Δp_x is the change of x momentum from the beginning to the end of the period:

$$\sigma_{zz}=\frac{1}{\mu_0}\left(\int_0^{\mu_0}v_z d\mu\right)^2,$$

$$\sigma_{xz}=\alpha\left(-\frac{1}{\mu_0}\int_0^{\mu_0}v_z d\mu\int_0^{\mu_0}\mu v_x d\mu+\int_0^{\mu_0}v_x d\mu\int_0^{\mu}v_z' d\mu'\right),$$

$$\sigma_{xy}=\alpha\left(\int_0^{\mu_0}v_x d\mu\int_0^{\mu}v_y' d\mu'-\frac{\Delta p_x}{\mu_0}\int_0^{\mu_0}\mu v_x d\mu\right),$$

$$\sigma_{xx}=\alpha^2\left(-\frac{1}{\mu_0}\left[\int_0^{\mu_0}\mu v_x d\mu\right]^2-\int_0^{\mu_0}\mu v_x d\mu\int_0^{\mu}v_x' d\mu'\right.$$
$$\left.+\int_0^{\mu_0}v_x\int_0^{\mu}\mu' v_x' d\mu'\right),$$

$$\sigma_{zy}=\frac{\Delta p_x}{\mu_0}\int_0^{\mu_0}v_z d\mu,$$

$$\sigma_{yy}=(\Delta p_x)^2/\mu_0.$$

For the copper Fermi surface, Coleman *et al.*[10] made the approximation that all electrons on closed orbits are free carriers and also that the thickness of the closed orbit layers greatly exceeds that of the open orbit layers.

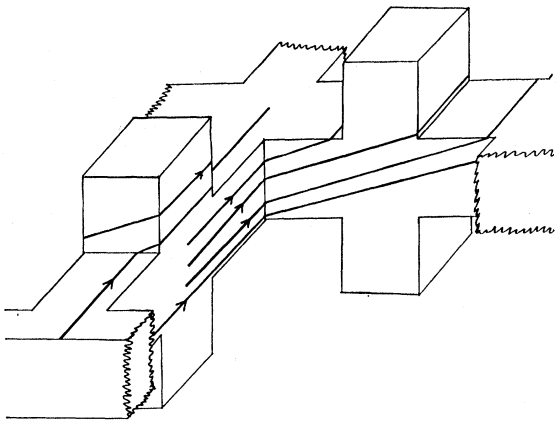

FIG. 14. Open and closed orbits on a logpile surface with the same topology as that of the fourth zone of the NFE model.

Then $\boldsymbol{\sigma}$ reduce to (orbits open in the x direction)

$$\boldsymbol{\sigma}=\begin{bmatrix}\sigma_{xx}(\text{F.E.}) & \sigma_{xy}(\text{F.E.}) & 0\\ \sigma_{yx}(\text{F.E.}) & \sigma_{yy}(\text{open}) & 0\\ 0 & 0 & \sigma_{zz}(\text{F.E.})\end{bmatrix}.$$

To determine the magnetoresistance, they calculated

$$\sigma_{yy}(\text{open})=(\Delta p_x)^2\int_{\text{B.Z.}}\frac{dp_z}{\mu_0}$$ and inverted $\boldsymbol{\sigma}$.

For the AuX_2 NFE surface we made three approximations.

(1) The fourth zone of the NFE model can be replaced by the "logpile" surface of Fig. 14 which has dimensions and topology like those of the NFE surface. Various types of open and closed orbits are illustrated.

(2) The necks in the third zone of the NFE model are pinched off. This approximation is equivalent to assuming that the thickness of the open orbit layers in the third zone is much less than the thickness of the open orbit bands in the fourth zone and also much less than the thickness of all closed orbit layers. dHvA results on the third-zone necks indicate that this approximation is a reasonable one.

(3) All carriers on closed orbits in the second, third, fifth, and sixth zones can be considered "free." This approximation only affects three of the six independent elements to $\boldsymbol{\sigma}$ in the high-field limit.

With these assumptions the expressions for the elements of $\boldsymbol{\sigma}$ given above were evaluated for $\mathbf{B}$ in {100}. The results of this calculation are given in Fig. 15. We use the convention $2\pi\hbar/a=1$, and $2e^2\tau/ma^3=1$. To determine ρ_{xx},

$$\rho_{xx}=(\sigma_{yy}\sigma_{zz}-\sigma_{zy}\sigma_{yz})/\det\sigma,$$

$$\det\sigma=[(\sigma_{yy}\sigma_{zz}-\sigma_{zy}\sigma_{yz})\sigma_{xx}+\sigma_{xy}\sigma_{zy}\sigma_{xz}+\sigma_{zx}\sigma_{yz}\sigma_{xy}$$
$$-\sigma_{xz}\sigma_{yy}\sigma_{zx}-\sigma_{zz}\sigma_{xy}\sigma_{yx}].$$

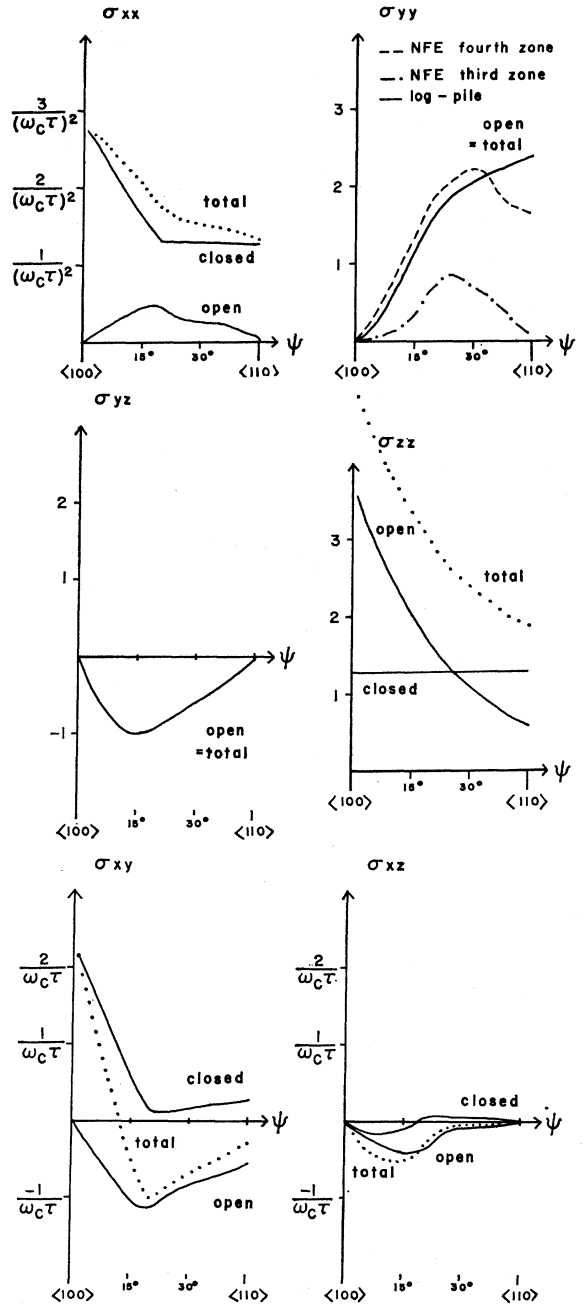

FIG. 15. Variation of σ with angle for the logpile model.

We note that both factors in the numerator are dimensionless, while all six factors in the denominator are given in units of $1/(\omega_c\tau)^2$. From Fig. 15 we can see then that all terms containing σ_{xz} or σ_{zz} will be small, and thus

$$\rho_{xx}\approx\frac{\sigma_{yy}\sigma_{zz}-\sigma_{zy}\sigma_{yz}}{(\sigma_{yy}\sigma_{zz}-\sigma_{zy}\sigma_{yz})\sigma_{xx}-\sigma_{zz}\sigma_{xy}\sigma_{yx}}.$$

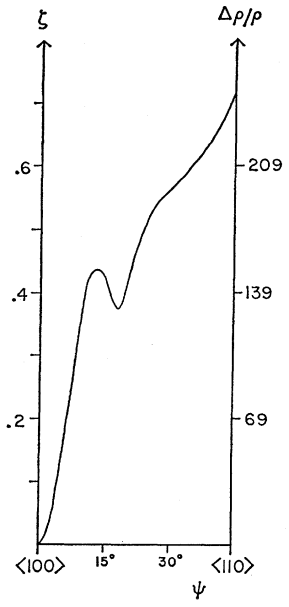

FIG. 16. ζ in {100} plane for logpile model.

We can estimate τ from the resistivity at $\mathbf{B}=0$ using a free-electron approximation, $\rho=ma^3/4ne^2\tau$. Here n is the number of conduction elections per primitive cell of volume $\frac{1}{4}a^3$. Then

$$\Delta\rho/\rho=2n\zeta(\omega_c\tau)^2-1,$$

where ζ is ρ_{xx} with the further reduction, $\omega_c\tau=1$. The value of $n=7$ for AuX_2. ζ is given in Fig. 16.

For $\mathbf{B}<5°$ from ⟨100⟩ in the {100} plane, ρ_{xx} is roughly proportional to σ_{yy}, which is in turn proportional to the thickness of layers of open orbits. This approximation is apparently only valid when a small fraction of the total number of carriers are on open orbits. This is the case for Cu.[10]

The fact that there is no dip in the experimental curves at $\psi\approx18°$ suggests that hole orbits persist on the real fourth-zone surface for several degrees beyond the 18° on the logpile model. Figure 15 shows why: σ_{xy} (closed) will then be larger, but $|\sigma_{xy}(\text{total})|$ will be smaller. Hence $\rho_{xx}\approx1/\sigma_{xx}$, unlike the model, resulting in a monotonic increase in ρ_{xx}. No pertinent dHvA data are available to aid in confirming this suggestion.

In addition to the complete calculation of $\boldsymbol{\sigma}$ for this model, we have determined σ_{yy} from the third- and fourth-zone open orbits of the NFE model. The results of that calculation, also shown in Fig. 15, indicate that the logpile model may be a farily good approximation to the NFE model and that the open orbits from the fourth zone do dominate those of the third zone even without the known reduction in the size of its copper-like necks.